SHIP-HELICOPTER OPERATIONAL LIMITATION ENVELOPE DEFINITION WITH CFD RESULTS AND WIND TUNNEL DATA

Caio Fuzaro Rafael*, Guilherme Araújo Lima da Silva*, Maurício José Machado Guedes**
***ATS – Aerothermal Solutions and Software Distributor, São Paulo, SP, Brazil**
**** CASNAV - Centro de Análise de Sistemas Navais –- Marinha do Brasil, Rio de Janeiro, RJ, Brazil**

Keywords: *SHOL, CFD, Wind Tunnel, Helicopter Landing Definition.*

Abstract

This paper presents a Ship-Helicopter Operational Limitation (SHOL) envelope definition based on a Computational Fluid Dynamics (CFD) study and on data from a wind tunnel campaign conducted at the Netherlands Aerospace Center (NLR) by the Brazilian Navy. The CFD study was done to fill gaps left by the wind tunnel campaign due to time and budget constraints. The experimental results were used to validate and calibrate the CFD simulation. Because wind tunnel data present only a few possible routes to the helicopter landing procedure, CFD simulation was used to construct other landing paths. The CFD solver used in this paper is CFD ++, which has precision performance and good prediction for aerodynamic flows. The results obtained were compared with the NLR tunnel data containing CFD results. The results obtained in the CFD simulations were considered satisfactory to be used in the determination of the helicopter landing process in ships. This will allow a fully automated process for determining SHOL through CFD results, with or without a few wind tunnel tests in the future. In summary, this paper presents a first attempt by the Brazilian Navy to determine SHOL with CFD results and wind tunnel data. In particular, the use of CFD in this method is done by few organizations around the world, such as NLR. This gives the Brazilian Navy the chance to implement a high technologyl process in order to cut costs as well as time in defining SHOL for its ships and helicopters.

1 Introduction

Helicopter operations are restricted by limitations established in the flight operation manuals of each helicopter. Typically, the operating limits involve aspects such as wind, altitude, or landing base slope, among others. The basic helicopter flight limitations are usually determined in a land-based environment by the aircraft manufacturer, but the more hazardous-prone ship operations require special procedures, which impose restrictions beyond those specified in flight manuals. These limitations are not supplied by the helicopter manufacturer, since they depend, to a large extent, on the specific class of ship involved and on its environment. The test campaign for defining operational limits, for launch and recovery of helicopters on board of ships or off-shore oil platforms, requires a step-by-step approach to guarantee the helicopter´s safe operation. The final result of such test campaign is the launch/recover envelope of that helicopter in the particular ship/platform considered as seen in other publications [1-4].

The typical steps in this campaign include:

- Study of the flow over the ship, and over the ship flight deck, using CFD simulation and wind tunnel testing;
- In situ measurements on the ship at sea to validate the simulations;
- Measurements of the helicopter over land to determine operational limits for its ship-borne use;

- Construction of a candidate flight envelope;
- Complete trials at sea to validate the candidate flight envelope.

Recent progress in CFD, as can be verified in previous works [5-8], provides the opportunity to compute the viscous, turbulent airflow over a surface combat ship and along the standard helicopter approach path in a time-accurate manner. Nevertheless, despite the improvement in CFD techniques, industry is still not prone to accept that the first item of the test campaign, enumerated above, could be performed solely using CFD simulations. Therefore, wind tunnel tests are still required to fully close the initial simulation phase of the test campaign. Furthermore, gradual substitution of wind tunnel tests by computational simulations also requires careful calibration and validation of the computational models. Therefore, in the present study, the computational results are compared to wind tunnel test data obtained at DNW-NLR site. Beyond the obvious validation of the present simulations, it is also expected that such comparisons will increase the reliability of the numerical model developed and, in the future, allow a decrease in the number of expensive wind tunnel test hours by replacing them with CFD simulations. The present study has used the CFD++, which was published in recent literature [9-11], a commercial CFD code (Metacomp Technologies, 2018).

2 Geometry and Tunnel Description

2.1 Geometry

The geometry used in wind tunnel testing campaigns and CFD simulations is that of Corvette Barroso V-34, which for the wind tunnel tests was prototyped in wood with details in 3D printing by the NLR team.

The model has a scale of 1/75, so the length of the ship is 1.38 m and it was built from the water line, i.e., with a flat section on the keel of the ship.

2.2 NLR Experimental Setup

The test was performed in the Low Speed wind Tunnel of NLR, an atmospheric wind tunnel of the closed return type. The velocity in the test section is about 30 m/s. It is important to note that for this case, the Reynolds similitude with sea operation is not necessary because the most important factor is the recirculations, not the effect of the viscous boundary layer.

The tunnel is equipped with an interchangeable aeronautical test section and a fixed nonaeronautical test section. The interchangeable test section is 3 meters wide and 2.25 meters high and has a length of 5.75 meters. Downstream of this interchangeable aeronautical test section is the fixed non-aeronautical test section with a length of 3 meters.

Each test section is equipped with a turntable, which is flushed into the floor of the test section. The diameter of the turntable in the non-aeronautical test section equals 2.40 m. The test section was equipped with a traversing beam that spans the width of the test section. The beam is equipped with a 5-hole pitot tube. The 5 pressures of this probe were combined to obtain the local flow velocity vector. The center of the flight deck is aligned with the center of the turntable and the probe pressure was registered at each degree.

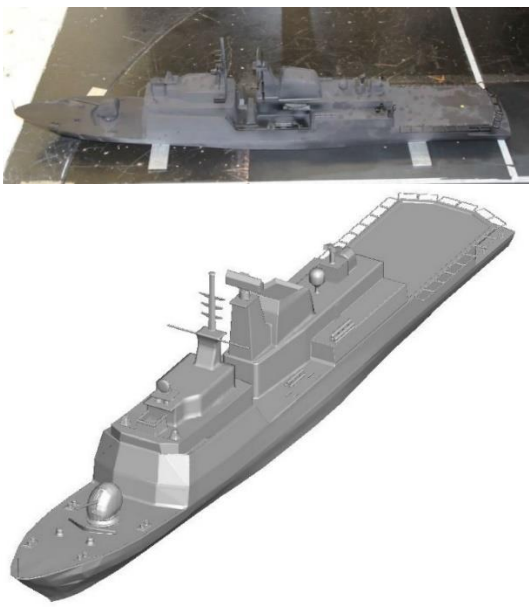

Fig 1. Model of the wind tunnel and CFD in the scale of 1/75.

The wind tunnel airflow measurements were made in 9 points, namely:

- Point 4, at four different heights: 3, 5 and 10 m above the flight deck in terms of actual full scale;
- Points 20, 30, 40, 50 and 60 at 10 m above the flight deck in terms of actuall full scale;
- Two measurements in: starboard and port ship anemometer position.

Fig. 2 and 3 show the positions of the 5-hole pilot tube in the wind tunnel test.

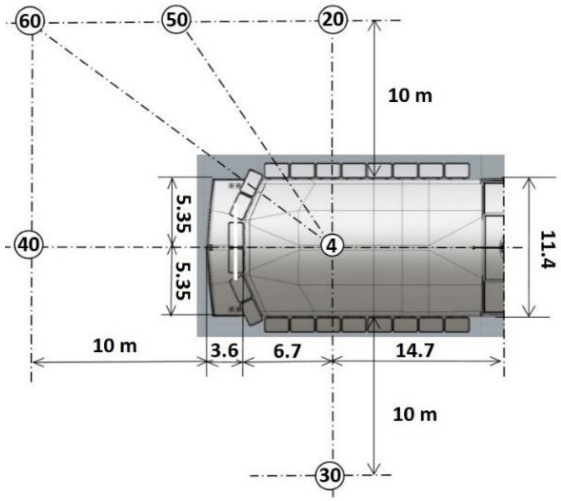

Fig 2. Positions of measuring stations above helicopter flight deck, distances full scale expressed in m.

One valuable piece of information about NLR wind tunnel is that the boundary layer on the floor of the non-aeronautical test section has a thickness of around 0.15 m.

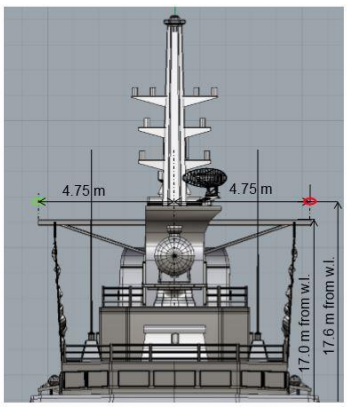

Fig 3. Positions of measuring stations, starboard ship anemometer (green) and port ship anemometer (red). Distances in real full scale expressed in m.

2.3 Wind Tunnel Data Reduction

In the full-scale situation, the relative wind vector is the resultant of the ship's speed and of undisturbed true wind velocity vectors. The wind tunnel directly generates the relative wind: the relative wind speed and direction are given by V_{rel} and β_{rel} respectively, obtained from the tunnel reference data.

The local wind velocity (V_{loc}), horizontal flow deviation (χ_{loc}) and vertical flow deviation (φ_{loc}) at a given position are determined by the data obtained with the 5-hole probe. The local wind speed is expressed as a fraction of the relative wind speed by defining the coefficient:

$$Cv_{loc} = \frac{V_{loc}}{V_{rel}} = \frac{\sqrt{U^2+V^2+W^2}}{V_{rel}} \qquad (1)$$

And the horizontal and vertical flow deviations are defined by:

$$\chi_{loc} = -\cos^{-1}\left(\frac{\sqrt{U^2+V^2}}{V_{loc}}\right) \qquad (2)$$

$$\varphi_{loc} = \cos^{-1}\left(-\frac{U}{\sqrt{U^2+V^2}}\right) \qquad (3)$$

The measured local horizontal flow deviation is expressed as χ_{loc} and is a function of β_{rel}. The local horizontal wind direction with reference to the ship is expressed as β_{loc} and is calculated from:

$$\beta_{loc} = \chi_{loc} - \beta_{rel} \qquad (4)$$

A positive value of χ_{loc} indicates a deviation of the local wind towards larger $\beta's$. The local upflow φ_{loc} follows directly from the 5-hole probe measurement. The local conditions at the ship's anemometer positions are denoted with the subscript "an" as follows:

$$Cv_{an} = \frac{V_{an}}{V_{rel}} \qquad (5)$$

$$\beta_{an} = \chi_{an} + \beta_{rel} \qquad (6)$$

The up flow at the ship's anemometer position angle is φ_{an}.

To distinguish between port and starboard anemometer positions, the subscripts 'P' and 'S', respectively, are used.

For practical purposes it is convenient to couple all measured local flow properties at an

arbitrary position above the ship to the data measured at the ship's anemometer positions. For this purpose, the measured data is reworked with the equations:

$$Cv^* = \frac{V_{an}}{V_{rel}} \quad \left(= \frac{Cv_{loc}}{Cv_{an}}\right) \tag{7}$$

$$\chi^* = \beta_{loc} - \beta_{an} \quad (= \chi_{loc} - \chi_{an}) \tag{8}$$

Calculation of φ^* $(= \varphi_{loc} - \varphi_{an})$ is not relevant, as the anemometer systems applied on the ship do not account for vertical air flow angles. The asterisk-marked properties need to be calculated twice: once for the port and once for the starboard anemometer. The addition 'P' or 'S' defines correlation with the port or starboard anemometer system, respectively, e.g. '$Cv - P^*$'. The horizontal component and the vertical (up flow / down flow) component of V_{loc} are also presented. These components are expressed as velocity coefficients and are defined as follows:

$$C_{vv} = Cv_{loc} \cdot \sin\varphi \tag{9}$$

$$C_{vh} = Cv_{loc} \cdot \cos\varphi \tag{10}$$

3 Numerical Simulation

The numerical results were obtained using Reynolds-averaged Navier-Stokes (RANS) equations using CFD ++ software from Metacomp Technologies Inc. The adopted spatial discretization is the second order, with Minmod type TVD limiter and with a nodal type polynomial base; the temporal integration adopted is of the implicit type.

The boundary conditions applied are described below:

- Boundary condition type Inflow: Characteristics-based, 30 m/s and 288 K;
- Boundary condition type Outflow: Simple Back Pressure;
- Boundary condition type Wind tunnel wall and floor: adiabatic viscous wall;
- Ship: adiabatic viscous wall;
- Cylinder wall: overset mesh for rotation of the mesh of turntable where the ship is positioned.

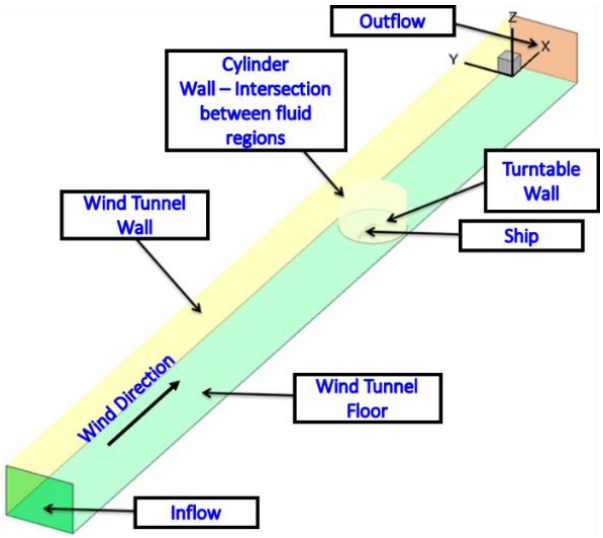

Fig 4. Families where the boundary conditions were applied.

3.1 CFD Preliminary Model

A preliminary CFD model was setup to study the mesh consistency and find the most appropriate mesh in terms of number of elements – or computational time – and accuracy. The compromise between time and accuracy was achieved with a mesh of 32.8 million elements that provided the best result for point 4, 10 meters from flight deck. This mesh gave -4% of error when compared to 40 million elements that gave an error of 3%.

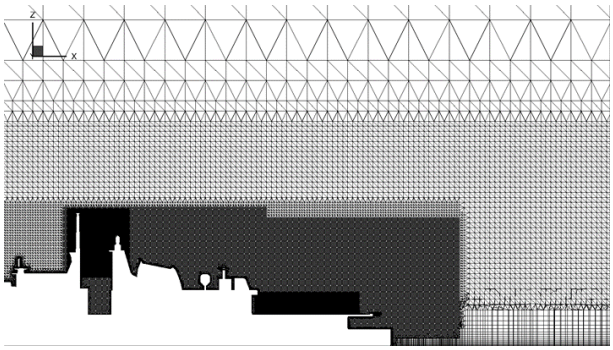

Fig 1. Detail of the mesh of 32.8 million elements, with the boxes of densities in the regions of interest.

The results are presented for normal velocity boundary conditions, and for the $\boldsymbol{k-\epsilon}$ turbulence model. It had the best results for points 20, 30, 40 and 60, since they have a smaller deviation of wind tunnel results when compared to the results obtained by the ***SST***

turbulence model. So, for all other CFD simulations the $\boldsymbol{k-\epsilon}$ turbulence model was chosen. The average error for $\boldsymbol{k-\epsilon}$ was -3% and for $\boldsymbol{SST}$ -4%.

After mesh and turbulence model were defined, the height of the boundary layer near the test body was studied. An entrance length and normal velocity to match the height of 0.15 m, as measured in the wind tunnel, was chosen. The details of preliminary computations were not included in the present paper due to space limitations. Other boundary layers were studied based on Musker turbulent profile from 75 to 150 mm. All of them resulted in larger deviations, > 7%, than normal profile at inlet surface.

3.2 CFD Final Model

As previously mentioned, the final model for CFD simulation has 32.8 million elements, the boundary condition for inflow is normal velocity, and the turbulence model is $\boldsymbol{\kappa-\epsilon}$ for the CFD. The simulations were made every 9º of yaw angle, and from the null yaw simulation, the mesh was rotated 9º degrees and was started from the previous solution, and so on, up to the 360º angle. These restarts of the simulations imply time savings but still guarantee quality of the results.

4 Validation Results

The following figures comparatively show the results obtained through the CFD simulations and the results of the NLR wind tunnel tests.

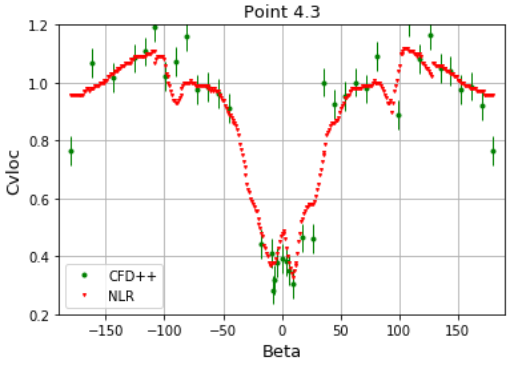

Fig 2. Cv_{loc} results for position 4, 3 meters above flight.

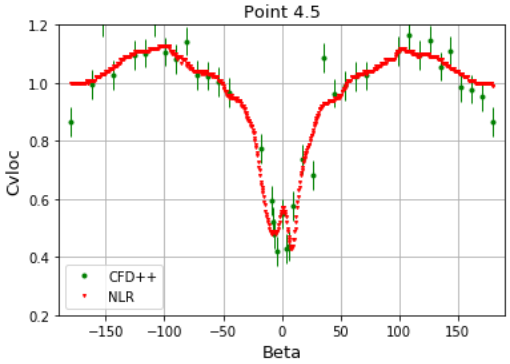

Fig 3. Cv_{loc} results for position 4, 5 meters above flight deck.

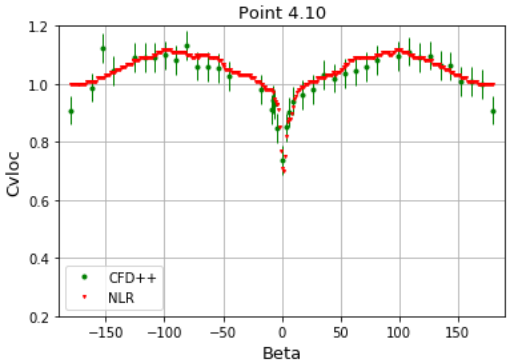

Fig 4. Cv_{loc} results for position 4, 10 meters above flight deck.

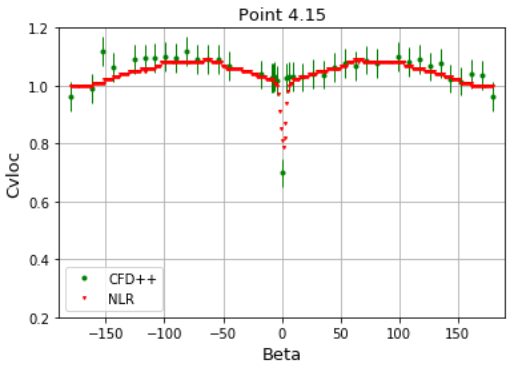

Fig 5. Cv_{loc} results for position 4, 15 meters above flight deck.

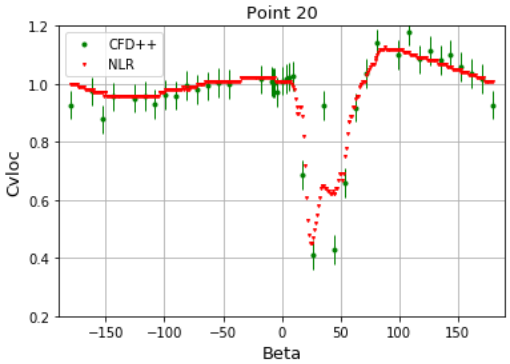

Fig 6. Cv_{loc} results for position 20, 10 meters above flight deck.

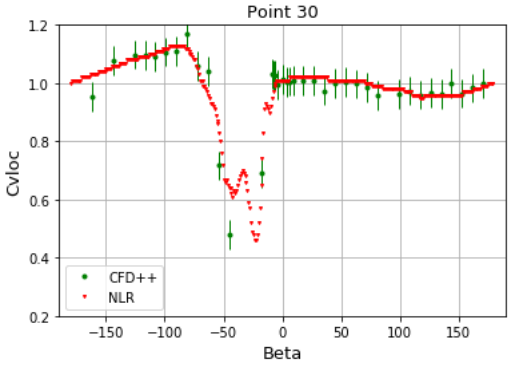

Fig 7. Cv_{loc} results for position 30, 10 meters above flight deck.

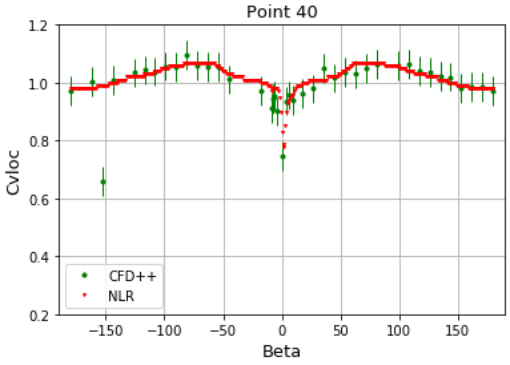

Fig 8. Cv_{loc} results for position 40, 10 meters above flight deck.

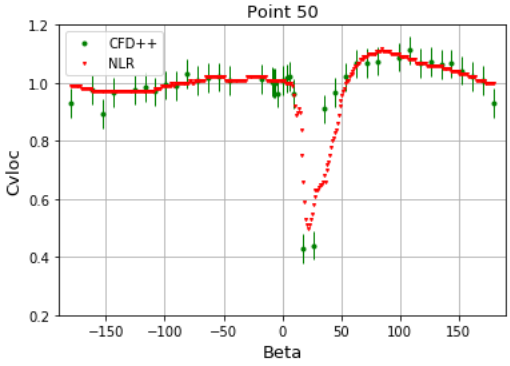

Fig 9. Cv_{loc} results for position 50, 10 meters above flight deck.

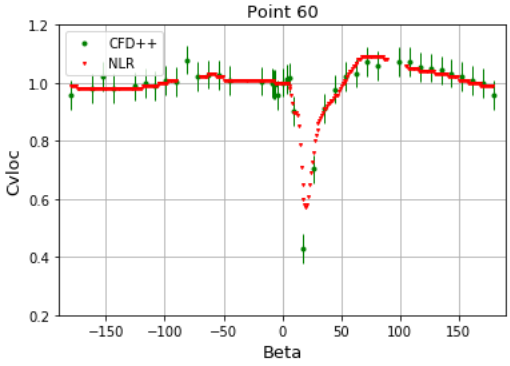

Fig 10. Cv_{loc} results for position 60, 10 meters above flight deck.

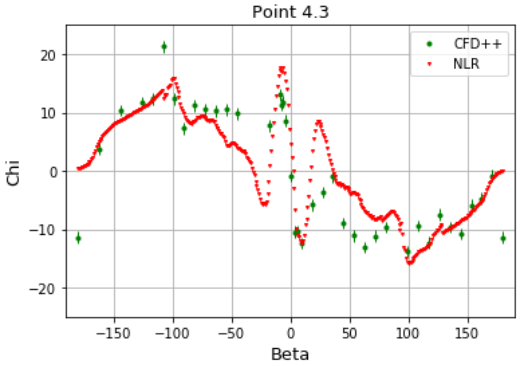

Fig 11. χ_{loc} results for position 4, 3 meters above flight deck.

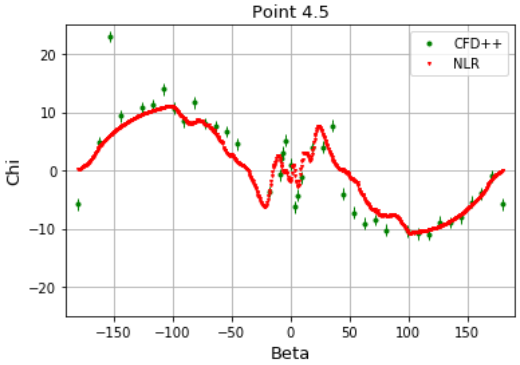

Fig 12. χ_{loc} results for position 4, 5 meters above flight deck.

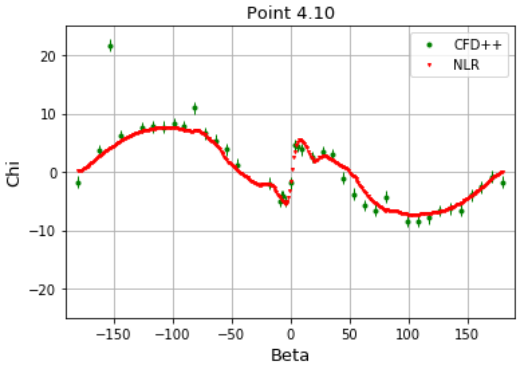

Fig 13. χ_{loc} results for position 4, 10 meters above flight deck.

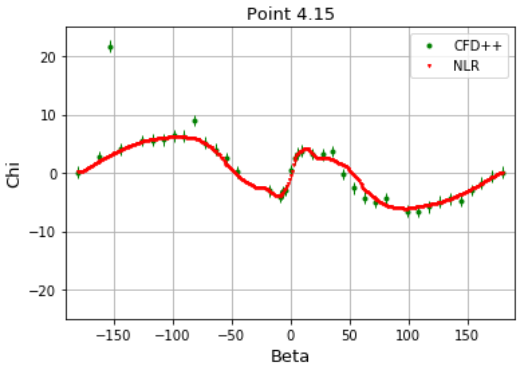

Fig 14. χ_{loc} results for position 4, 15 meters above flight deck.

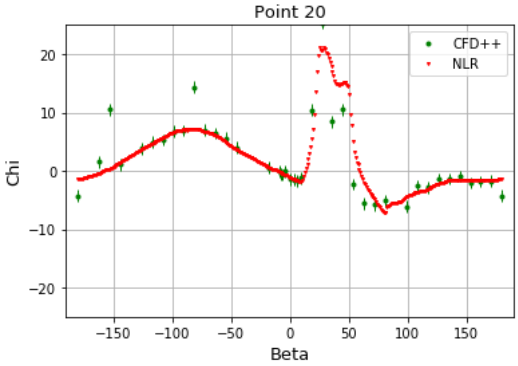

Fig 15. χ_{loc} results for position 20, 10 meters above flight deck.

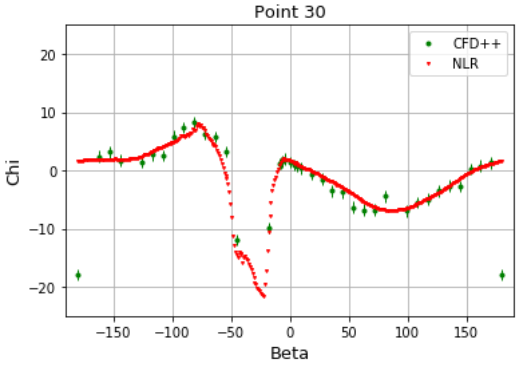

Fig 16. χ_{loc} results for position 30, 10 meters above flight deck.

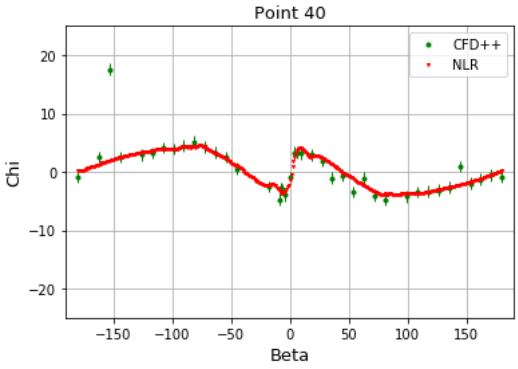

Fig 17. χ_{loc} results for position 40, 10 meters above flight deck.

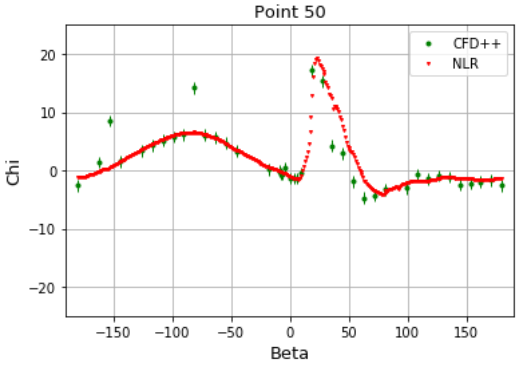

Fig 18. χ_{loc} results for position 50, 10 meters above flight deck.

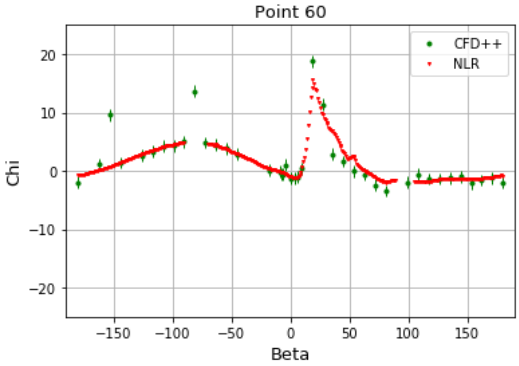

Fig 19. χ_{loc} results for position 60, 10 meters above flight deck.

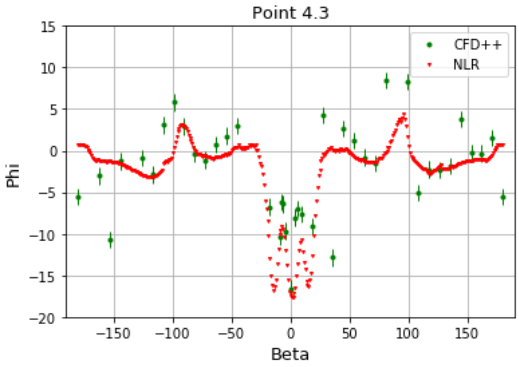

Fig 20. φ_{loc} results for position 4, 3 meters above flight deck.

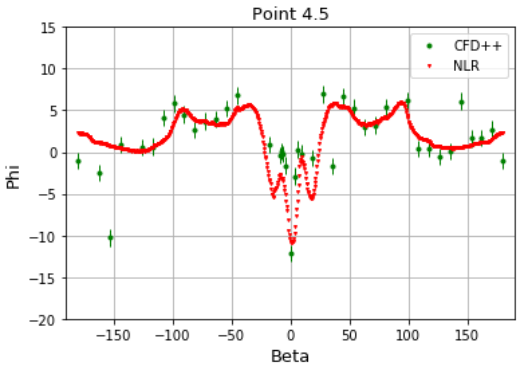

Fig 21. φ_{loc} results for position 4, 5 meters above flight deck.

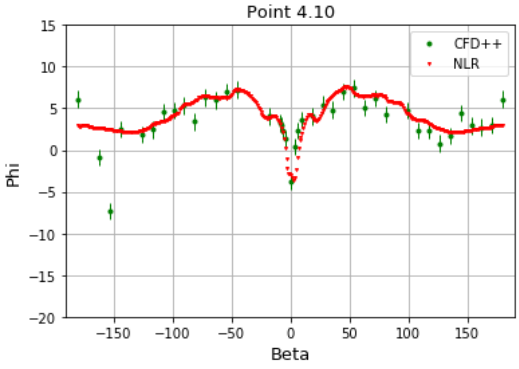

Fig 22. φ_{loc} results for position 4, 10 meters above flight deck.

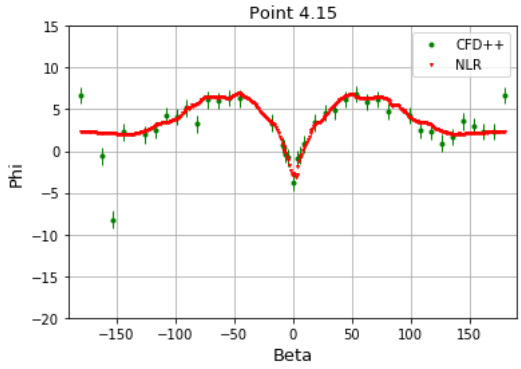

Fig 23. φ_{loc} results for position 4, 15 meters above flight deck.

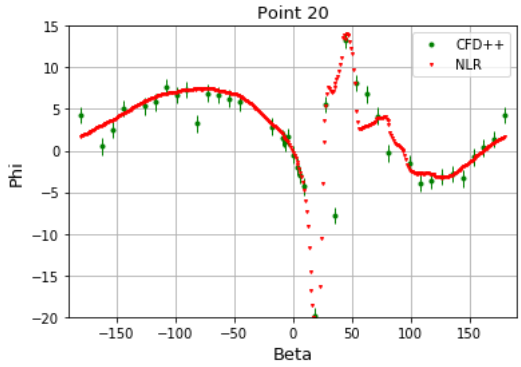

Fig 24. φ_{loc} results for position 20, 10 meters above flight deck.

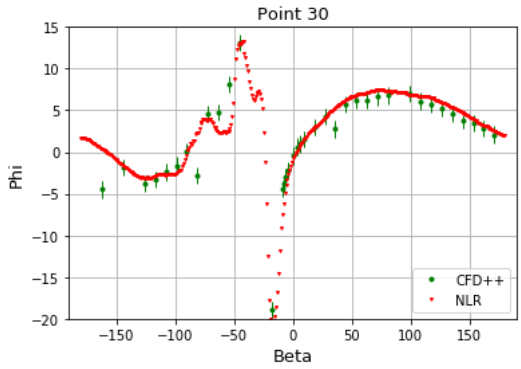

Fig 25. φ_{loc} results for position 30, 10 meters above flight deck.

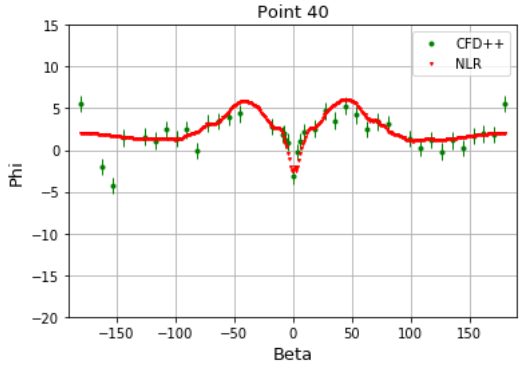

Fig 26. φ_{loc} results for position 40, 10 meters above flight deck.

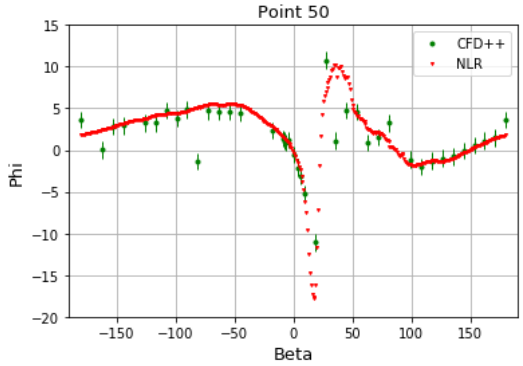

Fig 27. φ_{loc} results for position 50, 10 meters above flight deck.

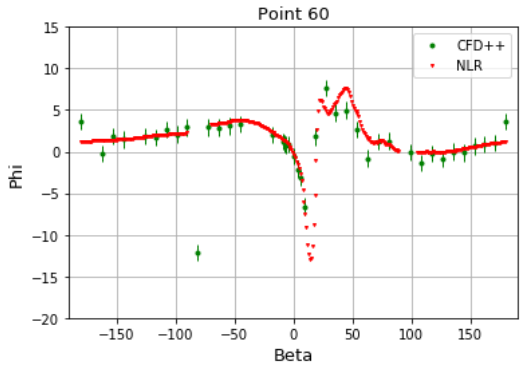

Fig 28. φ_{loc} results for position 60, 10 meters above flight deck.

Figures 1 to 10 are the results of the coefficients of velocities with an error bar of $\pm$ 0.05. Figures 11 to 28 are the results of horizontal and vertical deviations with an error bar of $\pm$ 1°.

5 SHOL Envelope Definition by CFD results

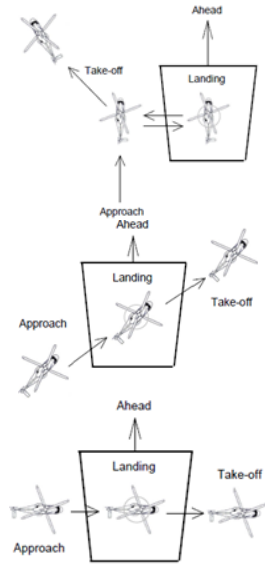

Fore-aft procedure

Oblique procedure

Cross-deck procedure

Fig 29.Helicopter Landing Procedures.

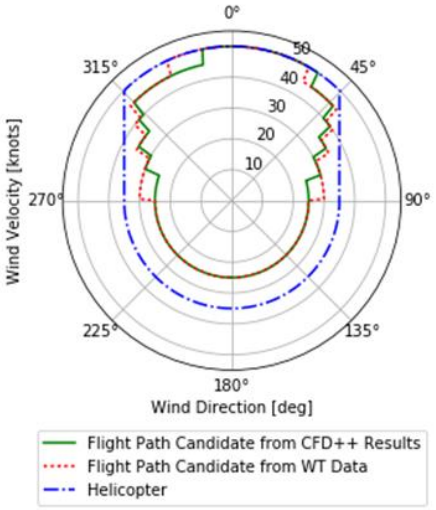

Fig 30. Fore-aft procedure passing through positions 60, 50, 20 and 4.

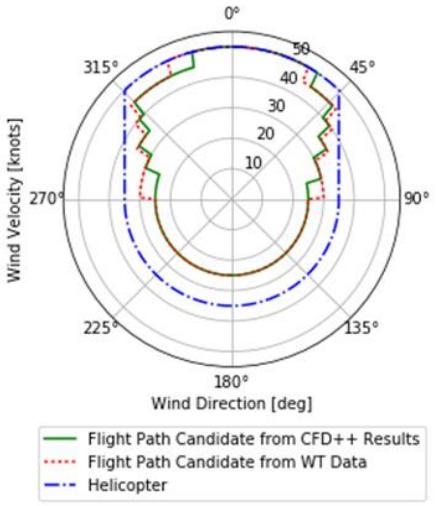

Fig 31. Oblique procedure passing through positions 60 and 4.

Figure 35 shows the helicopter path in relation to the ship studied in the present paper. Notice that the positions are not standard. The more common flight path was done with tunnel results directly, not by CFD.

Figures 36 to 39 present the flight envelope itself. It is a polar graph with helicopter angle and wind intensity. For the helicopter, the valid point is the lower intensity. The blue curve is the standard helicopter curve, the green represents CFD++ results and the red, the wind tunnel.

In general, CFD++ results were more conservative than wind tunnel results. Essentially, it is a good estimate, since you adopt an error bar that can comprise wind tunnel results without compromising the helicopter operation too much.

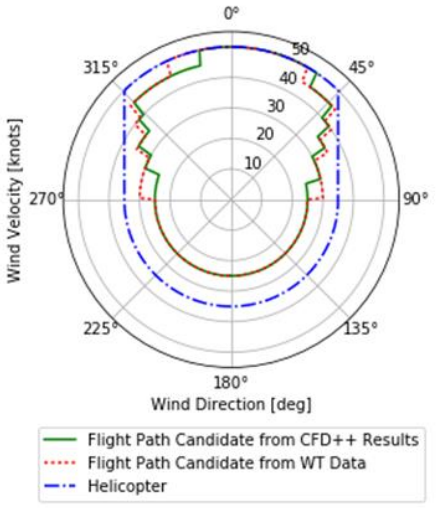

Fig 32. Oblique procedure passing through positions 50 and 4.

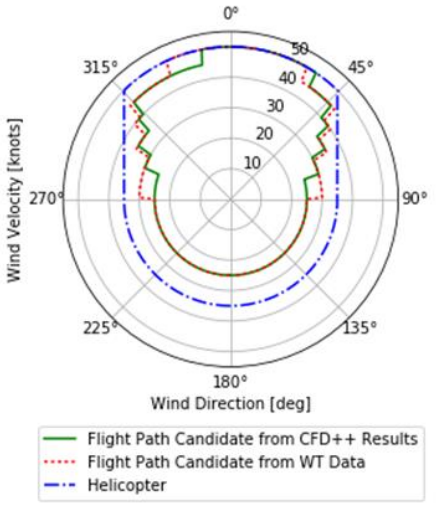

Fig 33. Cross-deck procedure passing through positions 20 and 4.

Figures 36 to 39 present the flight envelope itself. For the helicopter, the valid point is the lower intensity. The blue curve is the standard helicopter curve, the green represents CFD++ results and the red, the wind tunnel. The green line passed the red and blue lines. This is shown here only to have the full set of results presented here.

6 Conclusions

The point 4.03, point 4 at 3 meters from flight deck, is more difficult to match with the

Wind Tunnel Results for lower beta angles. The reason involves the reattachment and recirculation zones. CFD results of point 4.10 are closer to the Wind Tunnel Experimental Data. This point is very important in terms of accuracy because the Helicopter Landing Flight Envelope determination is largely dependent on point 4.10, point 4 at 10 meters of flight deck. The other points are matched with NLR data for all ranges of beta angles. Some spurious points, mainly at angles beta < -150 degrees, can be discarded and are due to mesh issues because the mesh was optimized for beta 0 degrees. In general, for flight envelope definition, CFD++ results were more conservative than wind tunnel results. It demonstrates that CFD results can be used to define a helicopter flight envelope to land on ships. Despite errors in local coefficients and angles, the flight envelope is less affected. In operational terms for the helicopter, CFD results are very close to wind tunnel results.

Acknowledgments

The authors would like to thank Diogo Mendes Pio, Guido Pires Arantes Ubertini and Pedro Castro Souza Villela from Aerothermal Solutions and Software Distributor for their support and advice. In addition, the authors would like to acknowledge Metacomp Technologies, CA, USA, for all the efficient support and inspiration.
The authors would like to thank Peter Booij from the National Aerospace Laboratory (NLR), Amsterdam, Netherlands, for his advice and support during the calculation of the SHOL methods.

References

[1] Hoencamp A. Helicopter Qualification Testing. “SHOL-X” Test Methodology. Ipskamp, 2016

[2] Hoencamp A. and Kruint V. Innovative Test Methodology for Helicopter-Ship Qualification Testing "SHOL-X" Test Methodology. 5th Asian/Australian Rotorcraft Forum 2016, p 1-13, 2016

[3] Hoencamp A. An Overview of SHOL Testing Within The Royal Netherlands Navy. Presentation. AHS Specialist Meeting Test & Evaluation, 2009

[4] Vorst J, Booij P, Hakkaart J. and Lee T. Qualification of KAI KUHKUH-1M on board Rokn ships using the dutch approach. 30th Congress International Council of the Aeronautical Sciences, Seoul, Korea, 2016.

[5] Sezer-Uzol N, Sharma A, and Long L. Computational fluid dynamics simulations of ship Airwake. Proc. IMechE Vol. 219 Part G: J. Aerospace Engineering, p. 369-92, 2005

[6] Forrest, J. S. and Hodge, S. J. and Owen, I. and Padfield, G. D. (2008) An investigation of ship airwake phenomena using time-accurate CFD and piloted helicopter flight simulation. In: 34th European Rotorcraft Forum 2008, ERF34, 16 - 19 September 2008, Liverpool, UK

[7] ShuklaSidh S, Singh S. and Srinivasan, B. A Computational Study of Modified TTCP/SFS Ship Airwakes. Conference: International Conference on Ship and Offshore Technology At: Khargpur, 2015.

[8] Scott, P. and Owen, Ieuan and White, M. (2014) The effect of ship size on the flying qualities of maritime helicopters. In: 70th American Helicopter Society International Annual Forum 2014, 20-22 May 2014, Montreal, QC, Canada

[9] Chakravarthy S. and Osher S. High resolution applications of the Osher upwind scheme for the Euler equations. In Proc. AIAA Computational Fluid Dynamics Conference, 6,1983, Danvers, pp. 363–373, AIAA Paper 83-1943

[10] Chakravarthy S., Peroomian O., Goldberg U and Palaniswamy S. The CFD++ computational fluid dynamics software suite. In Proc. World Aviation Congress & Exposition, 1998, Anaheim, Society of Automotive Engineers, 1998, SAE Paper 985564

[11] Goldberg U, Peroomian O, Chakravarthy S. A Wall-Distance-Free k-e Model With Enhanced Near-wall Treatment. ASME J. Fluids Eng.., v. 120, pp. 457-462, September 1998.

8 Contact Author Email Address

Caio Fuzaro Rafael, caio@ats4i.com.br
Guilherme A. L. da Silva, gasilva@ats4i.com.br
Maurício José Machado Guedes,
mauricio.guedes@marinha.mil.br

Copyright Statement